HEFAT2014
10th International Conference on Heat Transfer, Fluid Mechanics and Thermodynamics
14 – 26 July 2014
Orlando, Florida

COMPERATIVE ANALYSIS OF THE DI DIESEL ENGINE IN-CYLINDER FLUID FLOW APPLYING PIV MEASUREMENTS AND CFD SIMULATIONS

P. Dragomirov*, D. Buchtatyj, J. Sauerhering, J. Hadler, J. Schmidt, H. Rottengruber
*Author for correspondence
Institute of Fluid Mechanics and Thermodynamic,
Otto von Guericke University Magdeburg,
Magdeburg, 39106,
Germany,
E-mail: plamen.dragomirov@st.ovgu.de

ABSTRACT

To improve the efficiency of diesel engines several actions have been performed. Beside the reduction of internal friction by applying new and more effective materials, the thermodynamics offer different opportunities to influence the engine performance and emissions. Especially the interaction of fuel and air flow within the combustion chamber should be investigated. Therefore an optimized in-cylinder flow can enhance air-fuel mixing and lead to lower exhaust emissions and less fuel consumption. In addition the turbulent flow within the cylinder exhibits large- and small-scale cyclic variations[1]. The turbulence characteristics and cycle to cycle fluctuations of the in-cylinder flow can also have a pronounced influence on the combustion process and evoke the need to be thoroughly investigated.

Nowadays CFD simulations are widely used to predict and optimise the air flow within internal combustion engines, but such numerical calculations require a comparison with experimental data. Particle Image Velocimetry (PIV) was applied on an optically accessible single cylinder diesel engine to receive data sets for validation purpose. This engine provides access through a glass ring with 30 mm height and a modified piston bowl with an integrated glass bottom. In order to detect the local dependencies of the air flow, the velocity fields were quantified in two horizontal and three vertical measurement planes. A high resolution double shutter camera and a high energy double pulse laser were applied to measure the velocity fields during the intake and compression phases. In order to study the cyclic fluctuations, instantaneous snapshot pairs from 100 successive cycles were taken. As a result of the strong turbulences inside the internal combustion chamber strong cyclic fluctuations were observed at all investigated measurement planes.

The measured averaged in-cylinder velocities and indicated pressures were compared with a k-ε turbulence model simulation, based on an Unsteady Reynolds Averaged NavierStockes (URANS) approach. In addition, the swirl and tumble characteristics were calculated and checked against the measured ones. Despite a sufficient accordance between the experimentally determined and k-ε model calculated in-cylinder velocities, discrepancies in swirl and the tumble flow could be observed. Therefore the air flow was also simulated using a Scale-Adaptive Simulation (SAS) turbulence model in order to resolve the small scale turbulences inside the combustion chamber. The achieved solution was compared with the velocities fields, averaged over 100 cycles, as well as the single cycle velocities to avoid the elimination of small scale turbulences due to cyclic variations.

INTRODUCTION

To investigate the fuel-air-mixture and combustion process in internal combustion engines, it is useful to apply imaging techniques to an engine with optical accesses to analyse these processes [2]. The fuel-air-mixture depends on the atomization process [3] as well as on the air flow inside the combustion chamber [4, 5]. The air flow itself is highly influenced by the cylinder head and piston geometry. To analyse the air motion, complex and time consuming measurements are necessary. A geometrical optimisation process is only possible by creating expensive prototypes and therefore is based on a principal of trial and error. But if there is a possibility to accurately predict the behaviour of the airflow via computational methods, a geometrical optimisation will become much easier.

Even sophisticated numerical models, like SAS as shown in this publication, acquire experimental data to verify the used routines. With the aim of gaining data for validation of this numerical methods, an existing single-cylinder-optical accessible engine was used for detailed experimental investigations of the fluid flow.

NOMENCLATURE

CA	[°]	Crank angle
BDC	[-]	Bottom dead centre
MP	[-]	Measurement plane
PP	[-]	Piston position
TDC	[-]	Top dead centre
v	[m/s]	Velocity
VF	[-]	Vector field

Subscripts

max	Maximum

TEST RIG AND MEASUREMENT SYSTEM

Single-cylinder test bed

For the characterisation of the in-cylinder fluid flow velocities Particle Image Velocimetry (PIV) was employed on a single-cylinder research engine, see Figure 1. Its cylinder head, derived from a 4-Cylinder four-stroke diesel engine, has 2 intake and 2 outlet valves and a central position of the injector. The internal combustion engine has a relatively low compression ratio of 13:1, which is typical for research engines with wide optical accesses and therefore a voluminous piston top land. The optical access is ensured through a 28 mm high UV-grade fused silica liner positioned under the cylinder head and a modified piston bowl with a mounted flat glass window. The engine has a bore of 81 mm and a stroke of 95.5 mm and is laid out for engine speeds up to 3000 rpm and maximal cylinder pressure of 80 bar. It is also equipped with piezo-electric sensors in immediate proximity to the intake port and in the cylinder allowing a fine measurement of the pressure values (every 0.1° CA), which are sensitive input information for the computational simulations.

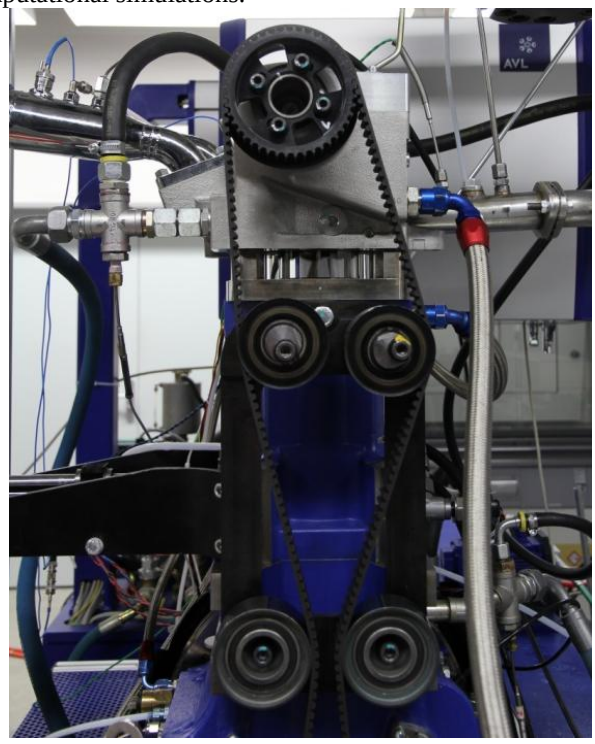

Figure 1 Single-cylinder research engine

PIV system

The PIV system "Flow Master D72" of LaVision (Goettingen, Germany) was employed in order to measure the air motion in the optically accessible diesel engine. It includes a LitronNano-PIV double pulsed laser, Imager ProX cameras, particle generator and control and analysis software (DaVis 7.2).

In order to visualise the air flow it needs to be seeded with suitable tracer particles, which were inserted at relatively large distance from the cylinder intake pipe. Shell hydraulic test oil was selected as a tracer and was nebulised with the air pressure based particle generator mentioned above. To assure a minimal slippage between tracer particle and airflow, the particle diameter needs to be quite small. On the other hand according the Mie-Theory, were the scattered light intensity is proportional to the droplet diameter, large particles are desired. As an optimum, a mean droplet diameter in a range of 3.0 µm was chosen and afterwards verified with a Dantec High-Dense 2D-PDPA System.

The seeded droplets were illuminated with a high-power low speed ND-YAG laser supplying pulses with energy of 300 mJ. It was linked with a flexible laser arm allowing the fine steering of the laser beam to the exact position in the combustion chamber. Due to the built-in deflection mirrors the laser beam has a lower energy on exit of the laser arm approximately 200/220 mJ. Afterwards focusing and meniscus cylindrical (-50f) lenses were mounted and thereby an about 1 mm thick laser sheet was achieved.

The double shutter Imager ProX camera was used in combination with a 135 mm Nikkor objective for the detection of the scattered Mie signal from the tracer droplets. This telephoto lens has a small image section capturing only the area of interest, the combustion chamber. The camera has a 1600 x 1200 resolution and a maximal acquisition frequency of 17.5 Hz.

MEASUREMENT PLANES AND ANALYSIS METHODS

In order to provide sufficient information for the validation of the CFD simulations, horizontal as well as vertical measurement planes were investigated. The experiments were conducted at 1500 and 2000 rpm during the intake and compression phases.

Horizontal measurement planes

Two dimensional measurements of the air flow velocities were done at two horizontal planes. To fully take advantage of the optical access of the liner, the two horizontal laser sheet planes were positioned at the top of the glass ring at 15° CA to avoid light deflection from the nozzle tip and at the deepest possible point at 55° CA, see Figure 2. To acquire the scattered light from the tracer particles the double shutter camera was aligned at the 45° mirror in the elongated cylinder viewing through the piston glass bottom, see Figure 2. Based on the flow velocities the pulse width was varied from 5 to 20 µs at

different CA positions during the intake and compression phases.

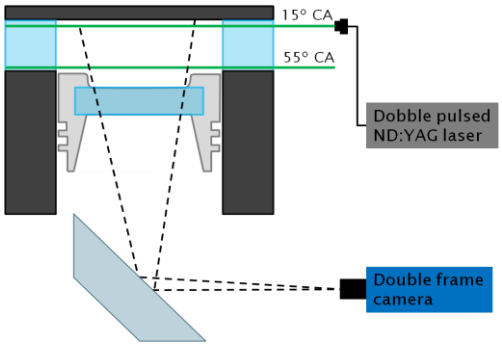

Figure 2 Experimental setup for the horizontal planes

Before the vector field calculations can be started several actions were undertaken to ease the whole process. Firstly background images without tracer particles taken previous to the experiments were subtracted in order to reduce the background noise and the reflections caused by the intake valves crossing the laser beam (in case of the 15° CA plane) and such due to scattered light from the cylinder head in general, see Figure 3. Secondly a round mask was used, so that the same area can be used for the calculations at all measurement times and in addition the necessary calculation time was reduced. Processed images from both horizontal measurement planes can be seen in Figure 4.

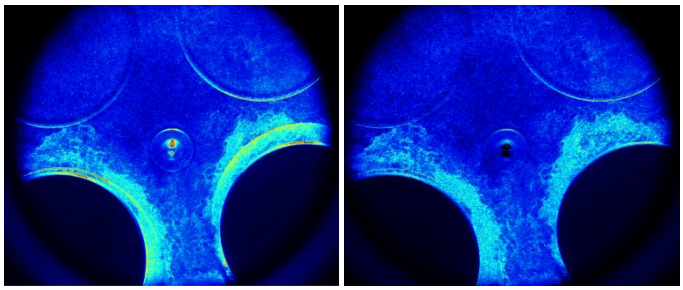

Figure 3 15° CA plane: raw (left) and after background subtraction (right) images

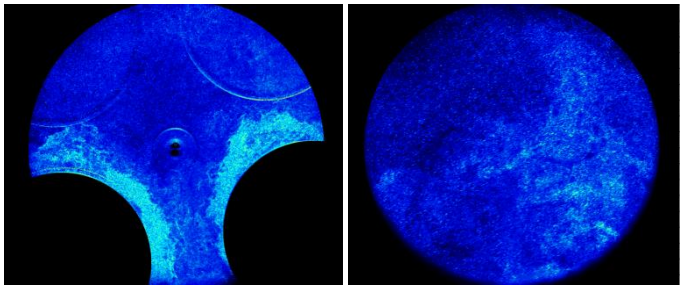

Figure 4 Processed images at 15° CA (left) and 55° CA (right) planes

In the pre-processing steps particle normalisation and sliding background were applied in order to increase the contrast of the droplets (between the droplets and the background). For the vector field calculations a multi pass cross-correlation with start grid of 64 by 64 pixels with 75% overlap and end grid of 32 by 32 pixels and 50% overlap was used. Velocity fields derived from one flow image pair using this method can be seen in Figure 5 for both investigated planes.

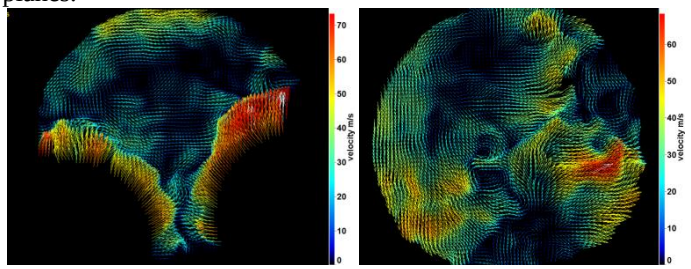

Figure 5 Vector fields at 15° CA (left) and 55° CA (right) planes

Vertical measurement planes

Velocity fields were also acquired by illuminating the inflowing tracer particles with vertical thin laser sheets at 3 different positions, in the middle of the two intake valves and in the centre of the cylinder, see Figure 6. The laser sheets were led in the combustion chamber through the glass ring, whereas in the case of the two planes in the centre of the intake valves the refraction on entry and exit of the glass liner needed to be accounted for, see Figure 6. A schematical illustration of the used experimental setup can be seen in Figure 6. Due to the distortion caused by the glass ring a 3D calibration plate was utilised in combination of the commercial software DaVis to correct acquired images.

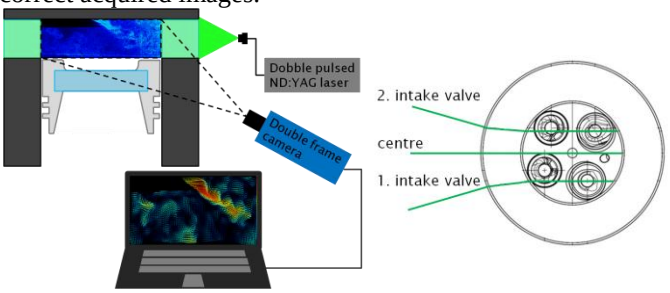

Figure 6 Experimental setup for the vertical measurement planes (left) and laser sheet positions (right)

Due to the strong reflections caused by the laser sheet crossing the glass ring several filtering techniques were executed in order to reduce them and in some cases they could be completely avoided, see Figure 7.

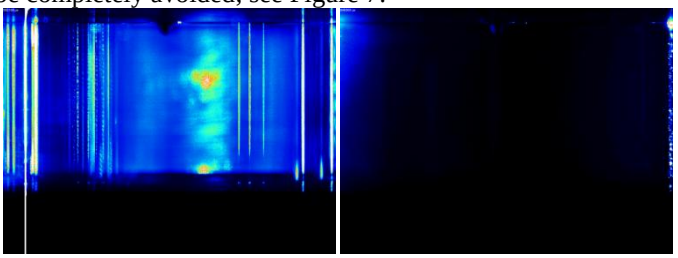

Figure 7 Vertical background image before (left) and after (right) filtering

The flow images taken at the different vertical planes went through the same processing steps, whereas different masks were used to define the area of interest for the vector calculations. In Figure 8 one processed flow image at intake valve 1 and the corresponding vector field can be observed.

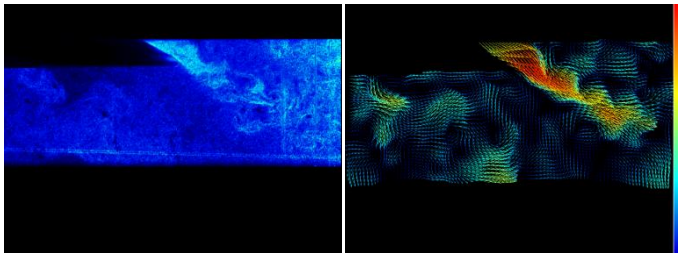

Figure 8 Flow image (left) and vector field (right) from the vertical plane at the middle of the 1. intake valve

NUMERICAL APPROACH

In order to investigate the influence of the turbulence on the in-cylinder flow, CFD simulations based on two different turbulence models were conducted. The numerical calculations for both models were built upon a 3D CAD model and the geometry meshing was created with the commercial software ICEM-CFD V15 (ANSYS Inc. Canonsburg, PA, USA). The simulations were executed using ANSYS-FLUENT V15 as a fast and stable solver. ANSYS-FLUENT as well as ParaView V:3.98.1. were applied during the post processing.

Model preparation

The simulations included the whole area from the intake port including the inlet manifold up to the outlet port. Figure 9 illustrates the negative model showing the geometrical boundaries for the airflow at bottom dead centre (BDC). Here the inlet manifold is to the left and is connected to the cylinder head with a screw joint.

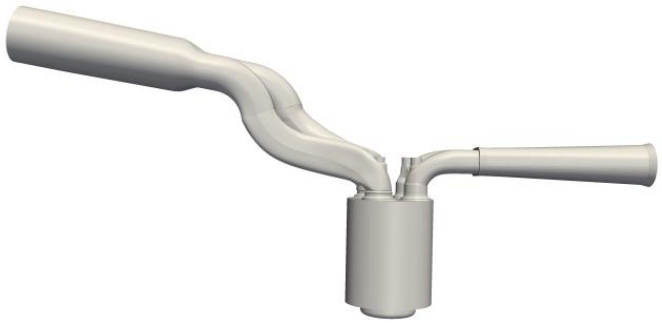

Figure 9 Negative model of the investigates area

The meshing process is significant to CFD simulations. Due to the complexity of the engine geometries as well as moving engine components a hybrid meshing method, combining hexa and tetra elements, was chosen. Figure 10 shows the generated mesh at top dead centre (TDC). The transient geometrical boundaries were modeled using layering, smoothing and remeshing [6].

Following the meshing, the fluid flow for the complete intake and compression phase was modeled. The high velocities correspond to high Reynolds numbers and leads to turbulent fluid flow. The numerical calculations were conducted using two different models to deal with turbulences. The first one is the realisable k-ε turbulence model combined with solving Unsteady Reynolds Averaged Navier Stokes (URANS) equations. The second model is a Scale-Adaptive Simulation (SAS). Its advantage consists in the ability to resolve even small scale turbulences, therefore allows the description of unsteady turbulent effects. With it also comes the disadvantage of increasing computation times depending on smaller meshing scales and higher temporal resolution. A more detailed description of the applied simulations can be found in [7].

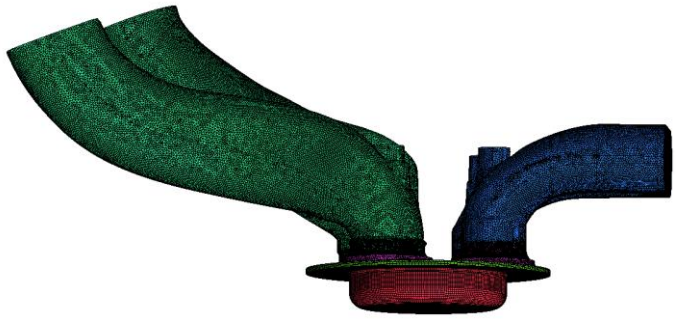

Figure 10 Generated mesh at TDC

RESULTS AND DISCUSSION

Qualitative comparison PIV/URANS

For each experimentally investigated duty point, 100 instantaneous snapshot pairs were recorded to ensure a high statistical probability. Afterwards averaged velocities were generated from those 100 repetitions and some of them are shown for the comparison in this section. The method 'sum of correlation' provided by the commercial software DaVis with the previously discussed options was used for this operation.

Horizontal planes

Due to the constricted view through the piston bowl a section from the cylinder at the horizontal planes was not visible for the double shutter camera. To ease the whole evaluation process of the generated vector fields the actual measurement area is roughly circled in.

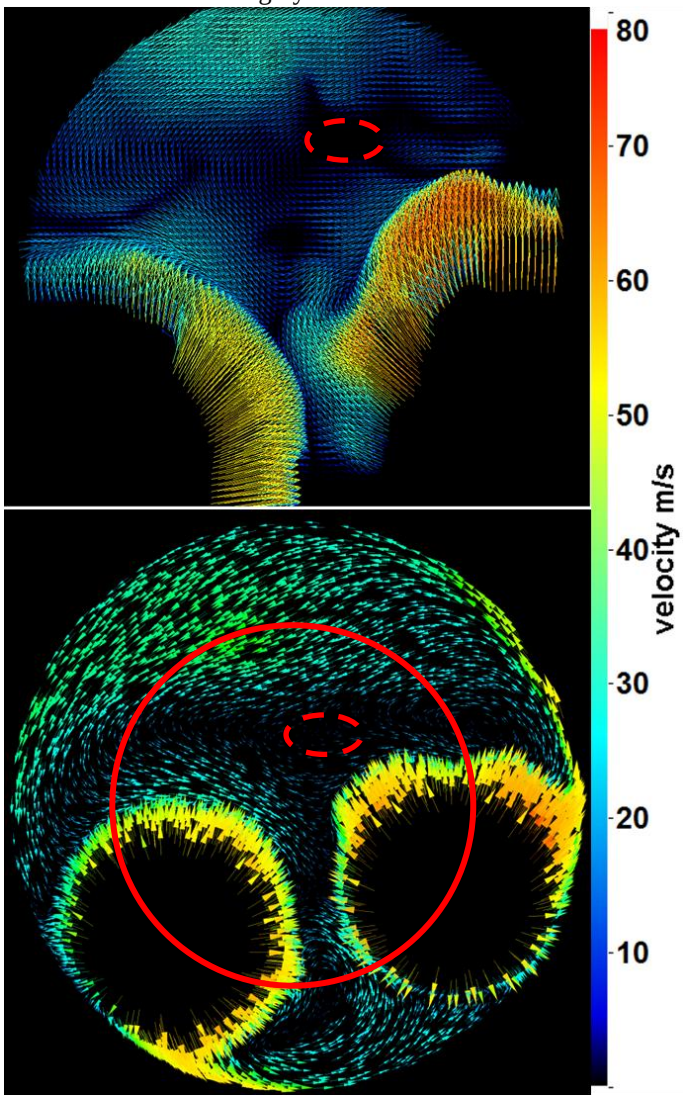

Figure 11 Experiment (top) and simulation (bottom) at measurement plane 15° CA and piston position 110° CA

In the case of the 15° CA MP small areas with absent vectors at edges of the valves and the nozzle tip conditioned by strong light reflections can be observed, see Figure 11 and Figure 12. In Figure 11 a comparison between experiment and simulation at 110° CA position, see Figure 2, is shown. Both techniques depict the inflow at the intake valves in a sufficient quality. The uneven inflow caused by the swirl intake canal and the cylinder head grinding near the valves can be seen by both vector fields and contributes to the developing of the swirl motion. At the valve to the right the air is been sucked in with higher pressure than at left one, which can be clearly observed by both velocity fields, and accelerated towards the cylinder wall generating an uniform flow along it. When the left valve has been reached, the air flow takes a fast turn towards the right valve and thereby generating a swirl motion at roughly the same spot for both measurement and simulation, see Figure 11. In general similar velocities of v_{max} near 65 m/s can be observed at the simulation in comparison to the experiment.

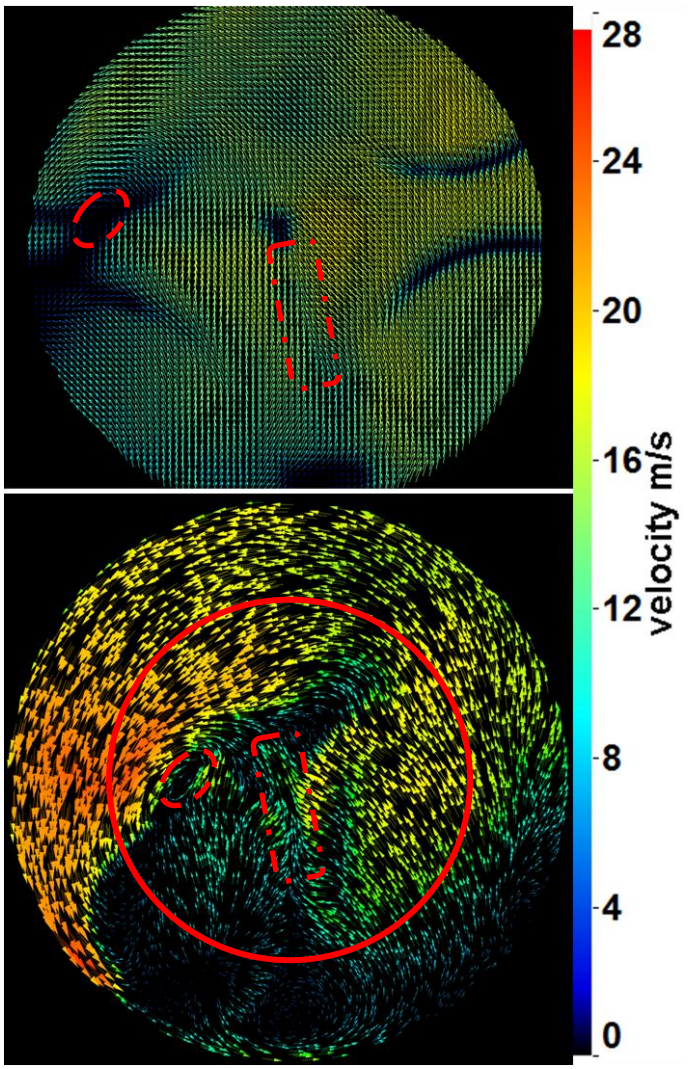

Figure 12 Experiment (top) and simulation (bottom) at measurement plane 15° CA and piston position 180° CA

Later on at BDC, see Figure 12, there are also similarities such as the small vortex to the left (circled in red) and the two flows intersecting in the centre (red rectangle). However the experimentally generated vector field appears more homogenous without strong pronounced inhomogenities.

The results for the lower measurement plane 55° CA are shown in Figure 13 - Figure 15 for different crank angle positions. At 60° CA the PIV imaging detected four vortex zones (red circled area) and generally high turbulence flow. In comparison to the CFD-results, where similar vortex regions can be observed, the inconsistencies with the experimentally acquired data are more significant. This indicates a nonsufficient consideration of the high turbulence at the early CA position for the CFD Model..

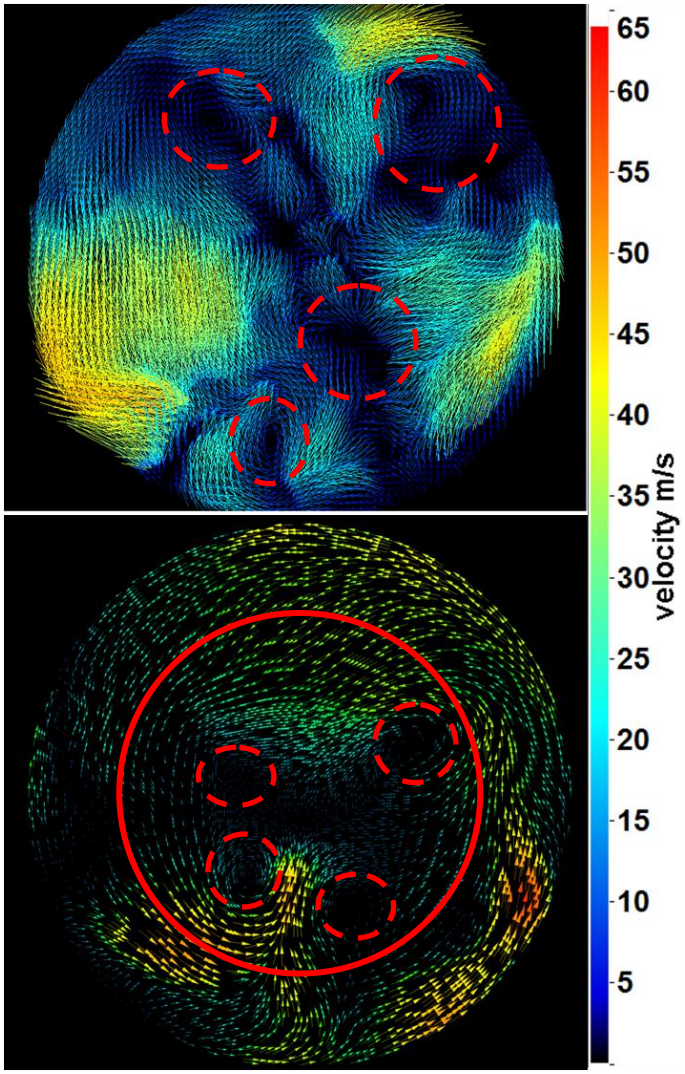

Figure 13 Experiment (top) and simulation (bottom) at measurement plane 55° CA and piston position 60° CA

For the later moment at 110° CA a good agreement between experiment and simulation is visible at Figure 14. The flow structures as well as the vector length are in a good accordance. The experimental determined dead zone, marked as red oval in the centre region and the two vortex zones at the top were recreated by the CFD. Even the maximum velocity zone at lower left in Figure 14 top can be found at nearly the same position.

At BDC, see Figure 15, the experimental data revealed a fully developed swirl motion with a single eye and maximal velocities beneath it. The vector field gained from the model shows a dual eye with a slightly more central position. A good agreement was achieved at zones with higher velocities.

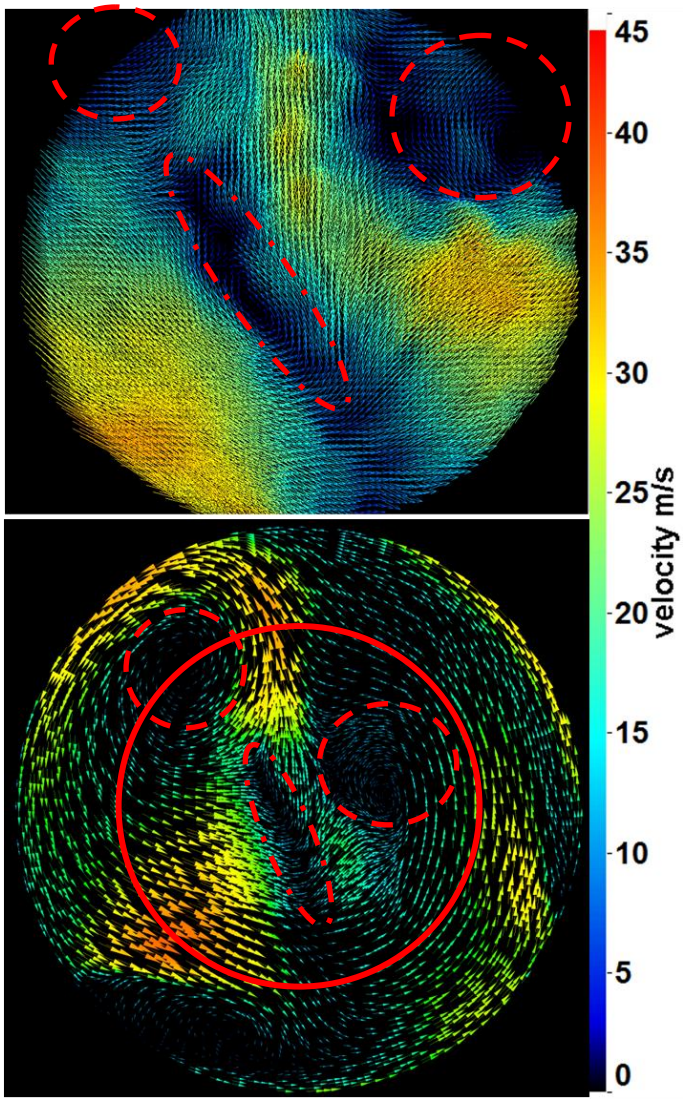

Figure 14 Experiment (top) and simulation (bottom) at measurement plane 55° CA and piston position 110° CA

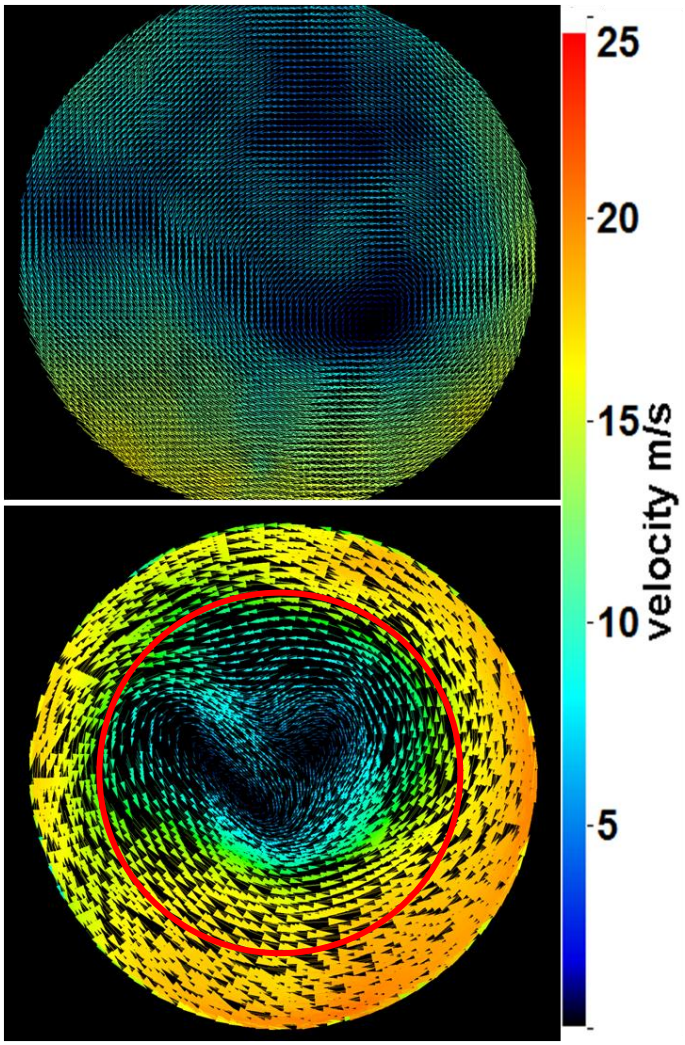

Figure 15 Experiment (top) and simulation (bottom) at measurement plane 55° CA and piston position 180° CA

Vertical planes

The intake valves intersect the laser sheets at the vertical measurement planes one and two, see Figure 6, and thereby cause a shadow to be cast behind them. Therefore the inflow from their left side was not visible for the camera and the corresponding velocity vectors are absent.

Some representative results from the vertical planes are shown in Figure 16 - Figure 19. The data was recorded at centres of both intake valves for two CA positions. The inflow as well as the following vortex structures can be found at both, experimentally and numerically obtained vector fields.

In Figure 16 at 50° CA where the valves have been barely opened, the velocity fields appear quite similar in qualitative and quantitative manner. Nevertheless the positions of the inlet jet streams and vortex regions are slightly shifted. In Figure 17 the experimental results show some higher inflow velocities, which causes a longer air jet stream and therefore the position of the vortex eye is shifted downwards.

At a later CA position 130°, see Figure 18 and Figure 19, an even better accordance can be seen. The same trend was observed for the horizontal planes, suggesting that the k-ε model is not able to accurately predict strong turbulences.

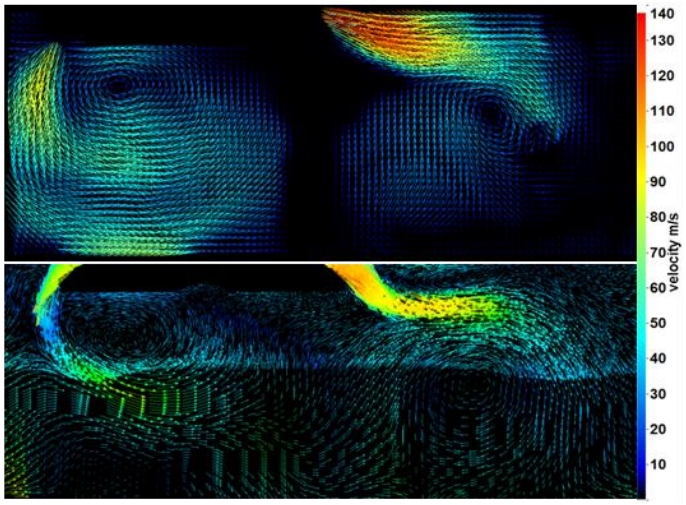

Figure 16 Experiment (top) and simulation (bottom) at measurement plane intake valve 1 and piston position 50° CA

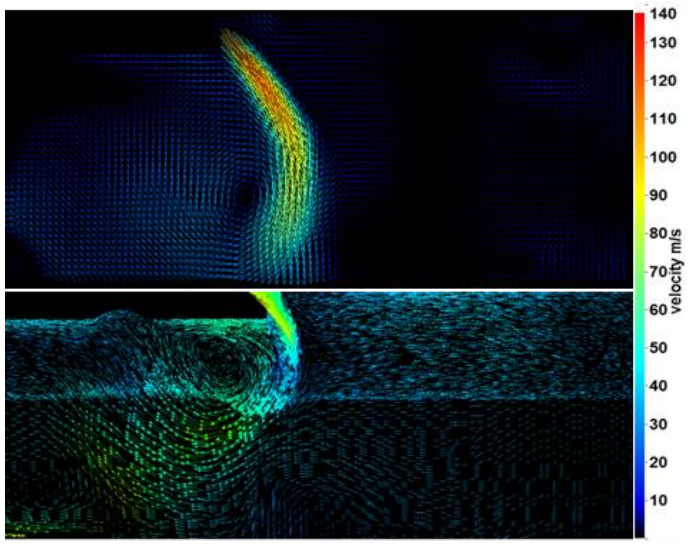

Figure 17 Experiment (top) and simulation (bottom) at measurement plane intake valve 2 and piston position 50° CA

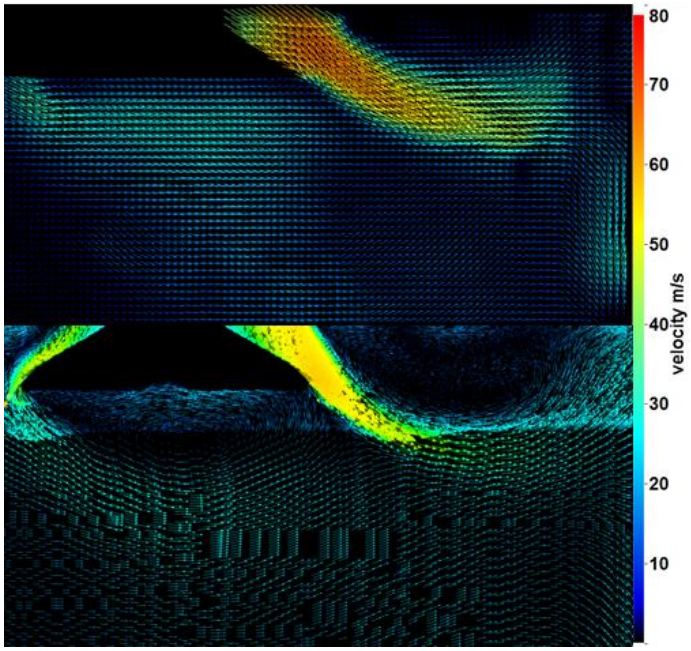

Figure 18 Experiment (top) and simulation (bottom) at measurement plane intake valve 1 and piston position 130° CA

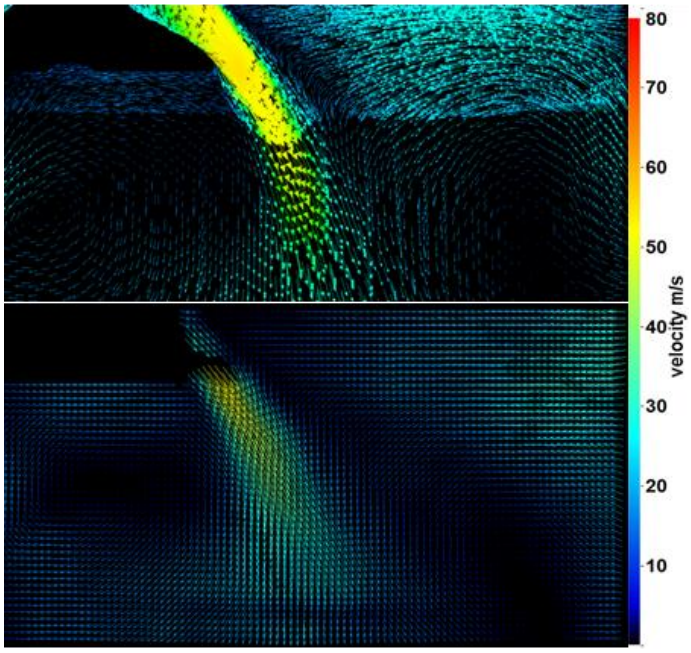

Figure 19 Experiment (top) and simulation (bottom) at measurement plane intake valve 2 and piston position 130° CA

Qualitative comparison PIV vs. SAS

Figures Figure 20 to Figure 23 show a comparison between experimentally acquired vector fields and results from the Scale-Adaptive Simulation.

In Figure 20 (top and centre images) it can be noticed, that the averaged vector field appears more homogeneous and in fact, there are only two large scale vortex structures distinguishable (circled in red, top image). In contrast to the experiment, the

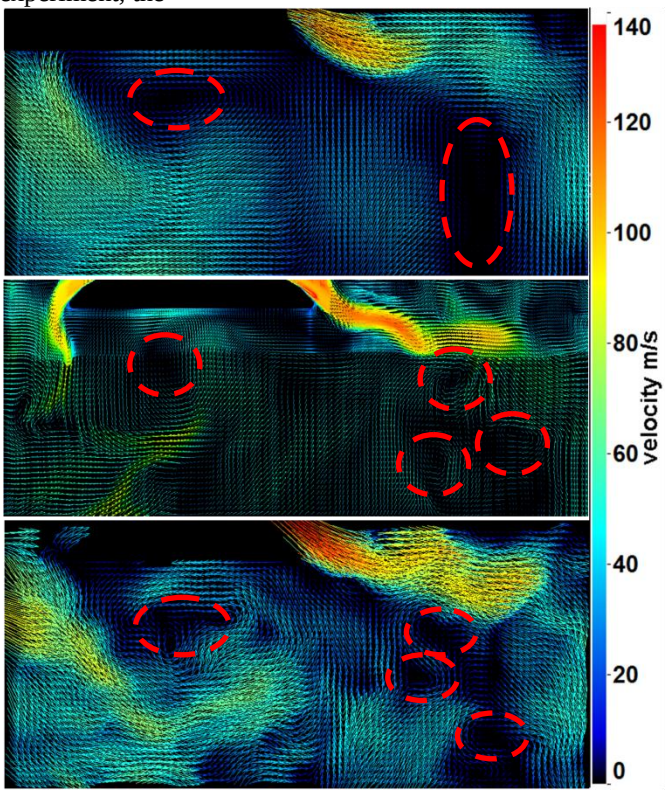

Figure 20 Averaged PIV velocity field (top), SAS (centre) and single PIV (bottom) at measurement plane intake valve 1 and piston position 60° CA

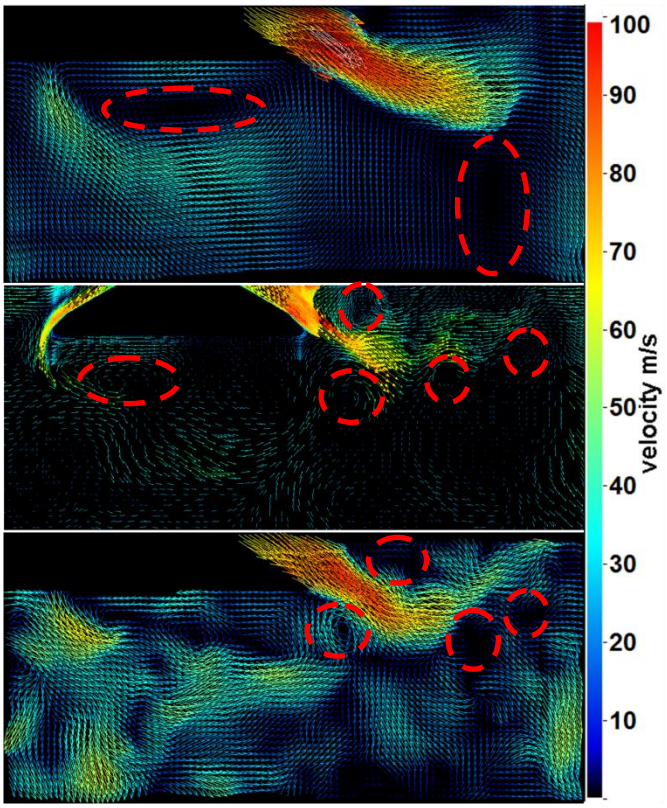

Figure 21 Averaged PIV velocity field (top), SAS (centre) and single PIV (bottom) at measurement plane intake valve 1 and piston position 90° CA

vector field gained from the simulation contains a relatively large vortex to the left and 3 small scaled vortex to right instead. In addition, the averaged velocities are smaller than the predicted ones from the SAS. This inconsistency can be contributed to the fact, that due to the vector field averaging, the small scaled turbulences and cycle to cycle fluctuations are being suppressed. Therefore to aid the comparison a vector field derived from a selected single cycle is shown, see Figure 20 (bottom image). This vector field is not only a better match concerning the flow turbulence and the vortex positions, also the velocities seem quantitatively more comparable. But nonetheless the non-averaged experimental results contain a various vector field characteristics due to the rather strong cyclic fluctuations. Therefore the similarity with the simulated field also varies between the different cycles.

Later on at 90° CA position, see Figure 21, a matching cycle could also be found and even the difference in the velocity magnitude is negligible. However the resemblance with the averaged vector field is unsatisfactory.

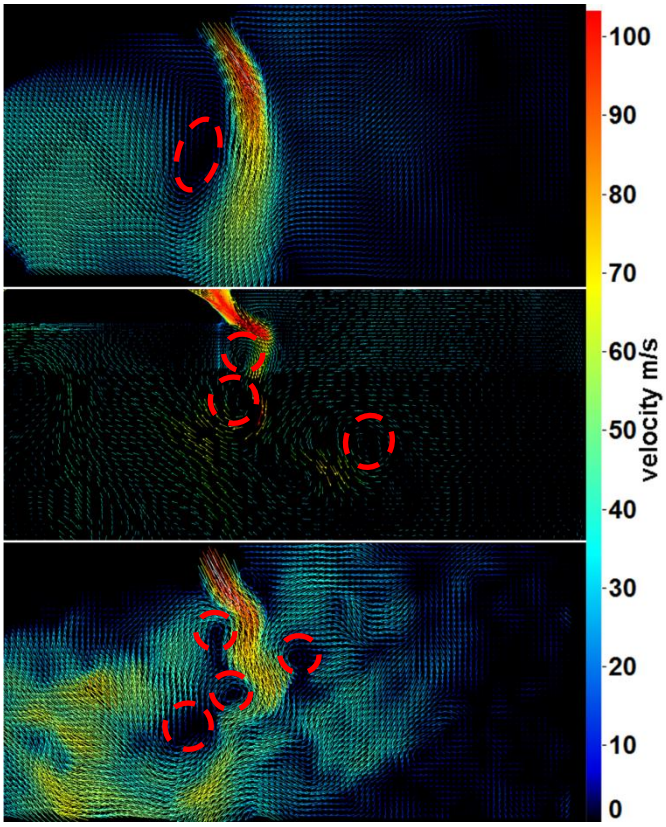

Figure 22 Averaged PIV velocity field (top), SAS simulation (centre) and single PIV VF (bottom) at measurement plane intake valve 2 and piston position 60° CA

In Figure 22 and Figure 23 the same CA positions are shown in the plane sight of the intake valve 2. The same trend concerning the simulation gained vector fields and the averaged and non-averaged PIV results can be observed. Whereas on the averaged PIV velocity fields, just a single vortex near the inflow is noticeable, the single PIV as well as the SAS vector fields contain considerably more vortex areas.

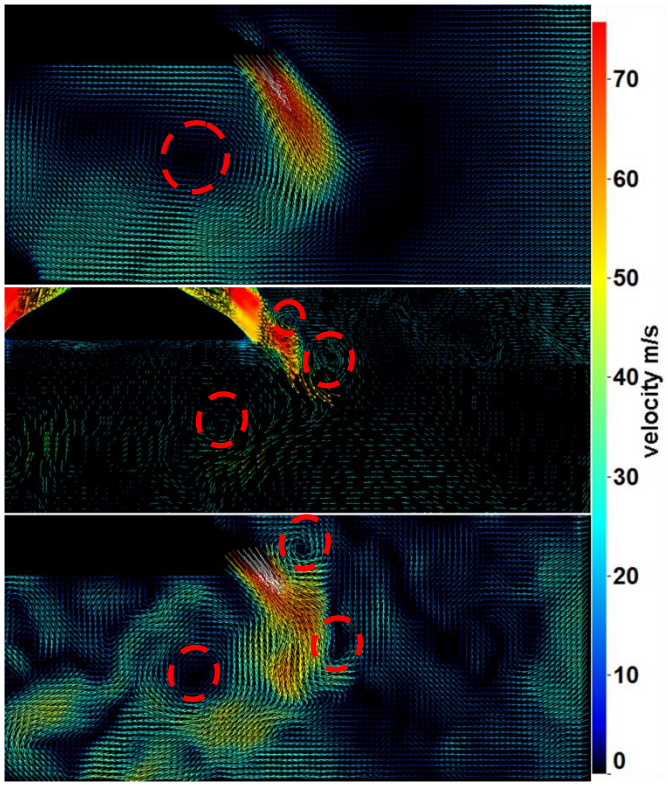

Figure 23 Averaged PIV velocity field (top), SAS simulation (centre) and single PIV VF (bottom) at measurement plane intake valve 2 and piston position 90° CA

CONCLUSIONS

Due to the high costs associated with the optimisation process of internal combustion engines there is a great struggle to achieve this goal with minimal possible experimental work. In that regard, a numerical simulation will be more suitable.

In order to develop an accurate and more reliable model for in-cylinder flow simulations, a single-cylinder optically accessible diesel engine was used to acquire experimental data for the validation process. PIV was applied to investigate the airflow motion at horizontal and vertical measurement planes. For the comparison between the experiments and the simulation results averaged PIV vector fields as well as non-averaged ones were used.

Firstly a more time efficient modelling tool, the k-ε model, was compared to averaged PIV velocity fields. On account of the simplicity of the computational model the qualitative accordance with the experimental results was satisfactory. Nevertheless, the model was not able to accurately predict the flow in detail and therefore, in some cases, the accuracy may not be suitable. This will be obvious in comparison to the non-averaged vector fields.

Secondly and more sophisticated method the Scale-Adaptive-Simulation was used. The method was able to compute more detailed vector fields, which in some cases show a good qualitative agreement with some of the non averaged PIV results.

Therefore it can be concluded, that in order to accurately compare this model to the experimental gained velocity fields more computations with variable boundary conditions are necessary. The variability results from the statistical behaviour of the measured pressure curve at the inlet channel, as well as the present flow field in the combustion chamber. Taking this into consideration, the results should be able to show the whole dynamic of the cyclic fluctuation captured by the experiments. It is also to be expected, that the average values from the computed fields are going to be comparable to the averaged experimental results.

ACKNOWLEDGEMENTS

I would like to thank the DFG and the graduate school 1554 for funding my research.

REFERENCES

1. Reeves, M., et al., *A high-speed all-digital technique for cycle-resolved 2-D flow measurement and flow visualisation within SI engine cylinders.* Optics and Lasers in Engineering, 1999. **31**(4): p. 247-261.

2. Dragomirov, P., et al. *Optical Analysis of High-pressure Injections in Transparent Engine*. in *European Conference on Liquid Atomization and Spray Systems*. 2013. Chaina, Greece: ILASS.

3. Backofen, D., et al. *Extreme Hochdruckeinspritzung alternativer Dieselkraftstoffe - Von der Kraftstoffeinbringung bis zur Emissionsbildung*. in *Diesel- und Benzindirekteinspritzung*. 2012. Berlin: Haus der Technik.

4. Huang, R.F., et al., *Topological flow evolutions in cylinder of a motored engine during intake and compression strokes.* Journal of Fluids and Structures, 2005. **20**(1): p. 105-127.

5. Huang, R.F., H.S. Yang, and C.N. Yeh, *In-cylinder flows of a motored four-stroke engine with flat-crown and slightly concave-crown pistons.* Experimental Thermal and Fluid Science, 2008. **32**(5): p. 1156-1167.

6. Colucci, P.J., et al., *In-Cylinder Engine Modeling Developments at Fluent*. 2002, Fluent Incorporation: Lebanon, NH.

7. Buchtatyj, D., et al. *Validierung einer CFD Simulation der Ansaugphase mittels optischer Messungen an einem Diesel-Transparentmotor*. in *Magdeburger Maschinenbau-Tage* 2013. Magdeburg.